



PERGAMON

Available online at www.sciencedirect.com

SCIENCE @ DIRECT®

Deep-Sea Research I 50 (2003) 1305–1321

DEEP-SEA RESEARCH
PART I

www.elsevier.com/locate/dsr

The thermohaline structure and evolution of the deep waters in the Canada Basin, Arctic Ocean

Mary-Louise Timmermans^{a,*}, Chris Garrett^a, Eddy Carmack^b

^aDepartment of Physics and Astronomy, University of Victoria, P.O. Box 3055 STN CSC, Victoria, BC, Canada V8W 3P6

^bInstitute of Ocean Sciences, P.O. Box 6000, 9860 West Saanich Road, Sidney, BC, Canada V8L 4B2

Received 10 August 2002; received in revised form 10 January 2003; accepted 23 June 2003

Abstract

Below the sill depth (at about 2400 m) of the Alpha-Mendeleyev ridge complex, the waters of the Canada Basin (CB) of the Arctic Ocean are isolated, with a ^{14}C isolation age of about 500 yr. The potential temperature θ decreases with depth to a minimum $\theta_m \approx -0.524^\circ\text{C}$ near 2400 m, increases with depth through an approximately 300 m thick transition layer to $\theta_h \approx -0.514^\circ\text{C}$, and then remains uniform from about 2700 m to the bottom at 3200–4000 m. The salinity increases monotonically with depth through the deep θ_m and transition layer from about 34.952 to about 34.956 and then remains uniform in the bottom layer. A striking staircase structure, suggestive of double-diffusive convection, is observed within the transition layer. The staircase structure is observed for about 1000 km across the basin and has been persistent for more than a decade. It is characterized by 2–3 mixed layers (10–60 m thick) separated by 2–16 m thick interfaces. Standard formulae, based on temperature and salinity jumps, suggest a double-diffusive heat flux through the staircase of about 40 mW m^{-2} , consistent with the measured geothermal heat flux of $40\text{--}60 \text{ mW m}^{-2}$. This is to be expected for a scenario with no deep-water renewal at present as we also show that changes in the bottom layer are too small to account for more than a small fraction of the geothermal heat flux. On the other hand, the observed interfaces between mixed layers in the staircase are too thick to support the required double-diffusive heat flux, either by molecular conduction or by turbulent mixing, as there is no evidence of sufficiently vigorous overturns within the interfaces. It therefore seems, that while the staircase structure may be maintained by a very weak heat flux, most of the geothermal heat flux is escaping through regions of the basin near lateral boundaries, where the staircase structure is not observed. The vertical eddy diffusivity required in these near-boundary regions is $\text{O}(10^{-3}) \text{ m}^2 \text{ s}^{-1}$. This implies Thorpe scales of order 10 m. We observe what may be Thorpe scales of this magnitude in boundary-region potential temperature profiles, but cannot tell if they are compensated by salinity. The weak stratification of the transition layer means that the large vertical mixing rate implies a local dissipation rate of only $\text{O}(10^{-10}) \text{ W kg}^{-1}$, which is not ruled out by plausible energy budgets. In addition, we discuss an alternative scenario of slow, continuous renewal of the CB deep water. In this scenario, we find that some of the geothermal heat flux is required to heat the new water and vertical fluxes through the transition layer are reduced.

© 2003 Elsevier Ltd. All rights reserved.

Keywords: Canadian Basin; Canada Basin (CB)

*Corresponding author. Woods Hole Oceanographic Institution, 266 Woods Hole Road, Mail Stop 21, Woods Hole, MA 02543, USA.

E-mail address: mtimmermans@whoi.edu (M.-L. Timmermans).

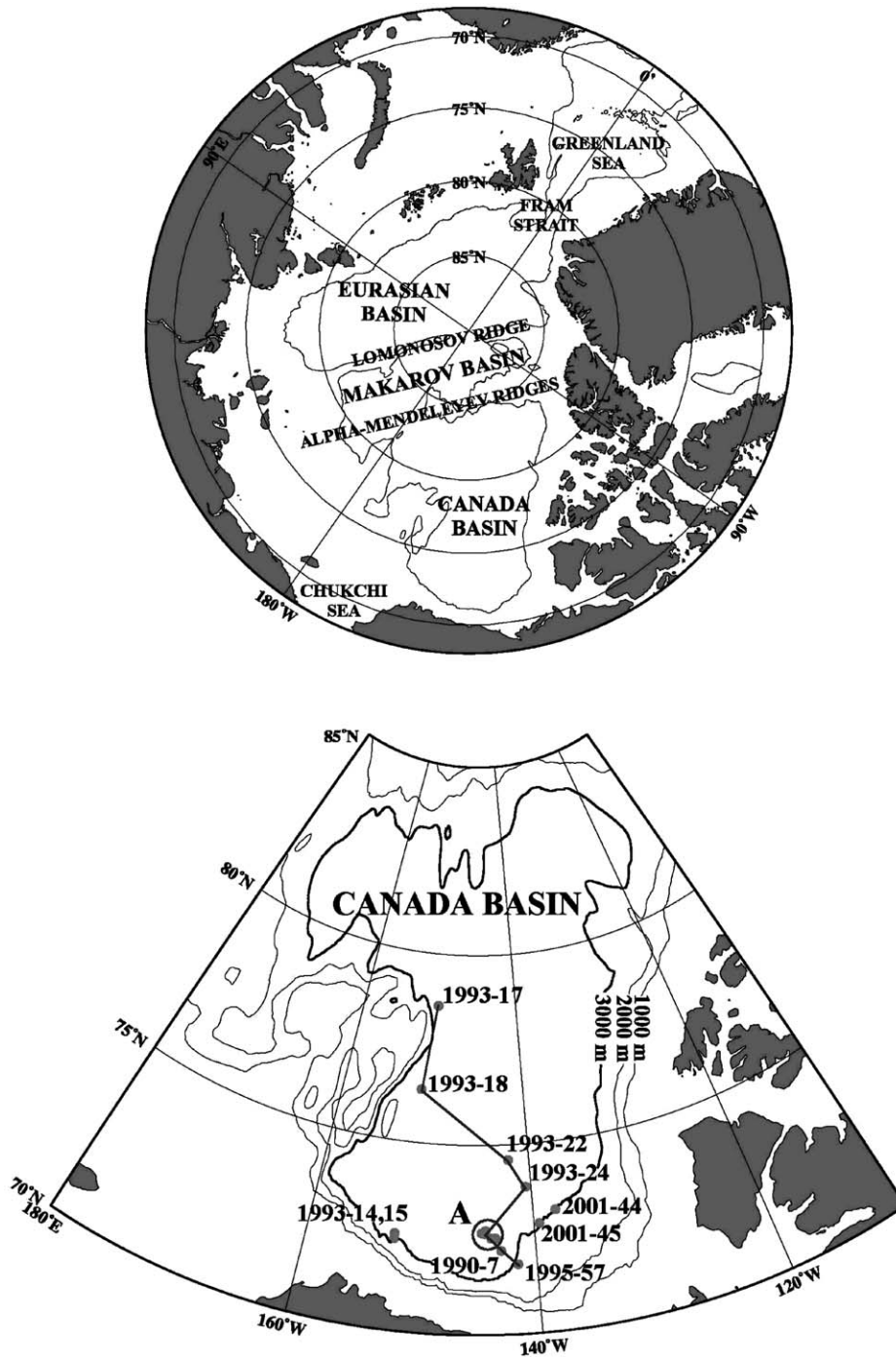


Fig. 1. Top: The Arctic Ocean. The Canadian Basin consists of the Makarov and Canada basins. Bottom: Deep station locations in the Canada Basin (CB) (labels indicate year-cast number). The circle at station A encompasses CTD casts: 1990–3, 1993–9, 1995–44, 47, 50. The line from 1993–17 to 1995–57 is the section shown in Fig. 3.

1. Introduction

The Arctic Ocean (AO) (Fig. 1) contains two main basins, the Eurasian and Canadian, separated by the Lomonosov Ridge with a sill depth around 2000 m, but with gaps in the ridge as deep as 2250 m (Perry and Fleming, 1986). There is direct deep-water exchange between the Eurasian Basin and the Norwegian and Greenland seas via Fram Strait (which has a sill at approximately 2600 m). The Canadian Basin on the North American side of the Lomonosov Ridge is isolated by this ridge and the deepest waters are either presently not being ventilated (Macdonald and Carmack, 1991; Macdonald et al., 1993; Aagaard and Carmack, 1994), or are being ventilated slowly with continuous renewal by shelf water (by freezing and brine rejection on the shelves) or influges from the adjacent Eurasian Basin (Aagaard et al., 1985; Östlund et al., 1987; Jones et al., 1995; Rudels et al., 2000). For the bulk of this paper, we will assume the no-ventilation scenario, but we will discuss the alternative in Section 7.

The deep waters of the Canadian Basin (below about 2200 m) are old, with a ^{14}C isolation age estimate of 450 yr (Schlosser et al., 1997). Schlosser et al. find no significant horizontal or vertical gradients in $\Delta^{14}\text{C}$ in the Canadian Basin below about 2200 m.

The Canadian Basin is separated by the Alpha-Mendeleyev ridge complex (with a sill at about 2400 m) into the Makarov and Canada basins (e.g. Swift et al., 1997). Of the AO basins, the Canada Basin (CB) has the largest volume and likely contains the oldest deep water (Macdonald and Carmack, 1991). Macdonald et al. (1993) hypothesize that the CB deep water is a relic of a renewal event that occurred around 500 yr ago, where this

effective deep water age is based on a one-dimensional diffusion model for ^{14}C . Aagaard and Carmack (1994) suggest, for example, that an absence of ice during summer would have resulted in the generation of dense water on the shelf the following winter, because of the reduced amount of fresh water on the shelf and also because of the large potential for new ice formation. Hence, a decrease in open water during summer around the rim of the CB about 500 yr ago could have ended the ventilation of the deep waters. Whatever the case, perturbations in upper ocean forcing may lead to altered vertical structure in the deep AO through changes in the continental run-off, or in ice production over the shelves. Because the CB deep waters are isolated both horizontally by the Lomonosov and Alpha-Mendeleyev ridges and vertically by stratification, it is possible to detect changes within them due to external fluxes (such as geothermal heating) from below. Here, we investigate the thermohaline structure of the CB deep waters, which we take to be deeper than about 2200 m.

2. Hydrographic observations

The conductivity–temperature–depth (CTD) data presented here were obtained in the southern CB between 1990 and 2001. Table 1 summarizes the expeditions, instrumentation and CTD casts; cast locations are shown in Fig. 1(b). Instrument accuracies were in the ranges ± 0.001 to 0.002°C for T , ± 0.002 to 0.005 for S and ± 2 m for D . Instrument resolutions were about 0.0003°C for T , 0.0002 for S and 0.2 m for D . Temperature and depth sensors were calibrated prior to and after each expedition. Salinity measurements were

Table 1

Canada Basin expeditions and CTD instruments used for deep measurements. Deep station locations for each year are shown in Fig. 1

Year	Ship	CTD instrument	Casts
1990	CCGS <i>Henry Larsen</i>	Guildline 8705	1990–3, 7
1993	CCGS <i>Henry Larsen</i>	Falmouth Sci. Inst. (FSI) ICTD	1993–9, 14, 15
1993	USCG <i>Polar Star</i>	SeaBird (SBE) 911	1993–17, 18, 22, 24
1995	CCGS <i>Louis S. St-Laurent</i>	FSI ICTD	1995–44, 47, 50, 57
2001	CCGS <i>Sir Wilfred Laurier</i>	SBE 25	2001–44, 45

calibrated with water samples analysed on a Guildline Auto-Sal salinometer. Potential temperature θ (referenced to the surface) and potential density σ were computed using the algorithms in UNESCO (1983).

CTD casts show the basic hydrographic structure of the CB to be as follows: a relatively fresh

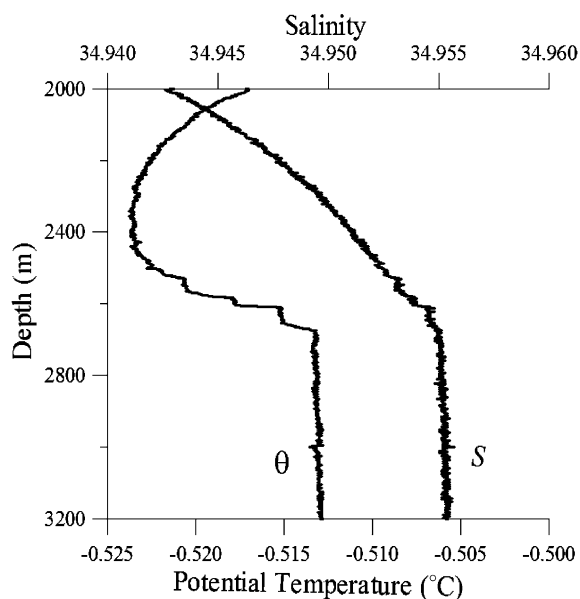


Fig. 2. Profiles of potential temperature (θ) and salinity (S) in the CB (cast 1993–24).

surface layer extending down to about 50 m (the Polar Mixed Layer), a strongly salt-stratified layer between about 50 and 400 m (the Halocline Complex), a relatively warm mid-depth layer of Atlantic origin (the Atlantic Layer) between about 400 and 1500 m, and cold deep layers extending from about 1500 m to the bottom.

The deep thermohaline structure of the CB is shown in Fig. 2. The potential temperature reaches a deep minimum $\theta_m \approx -0.524^\circ\text{C}$ at about 2400 m (the Alpha-Mendeleyev sill depth), increases with depth through a transition layer to $\theta_h \approx -0.514^\circ\text{C}$ at a depth of about 2700 m, and remains nearly constant to the bottom at 3200–4000 m. Salinity in the CB increases with depth to about 2700 m, but is nearly constant at about 34.956 below this depth (Table 2). Here we focus on the deepest water, which we refer to as the CB deep water, below the depth of θ_m .

Vertical sections of (a) θ and (b) S (Fig. 3) across the CB illustrate the lateral extent of the transition and bottom homogeneous layers. The transition layer lies between the depth of the potential temperature minimum and the top of the homogeneous bottom layer and has a thickness of about 300 m. Lateral gradients in θ within the transition layer appear only near the boundary of the basin. The homogeneous bottom layer has an average thickness of about 1000 m in the central CB.

Table 2
Characteristics of the deep CB

Cast	D_m (m)	H (m)	$\Delta\theta$ ($^\circ\text{C}$)	ΔS	θ_h ($^\circ\text{C}$)	θ_m ($^\circ\text{C}$)	S_m	S_h
1990–3	2440	260	0.010	0.0035	–0.515	–0.525	34.9540	34.9575
1990–7	2360	250	0.010	0.0035	–0.514	–0.524	34.9535	34.9570
1993–9	2450	345	0.010	0.0045	–0.509	–0.519	34.9520	34.9565
1993–17	2300	350	0.009	0.0040	–0.515	–0.524	34.9525	34.9565
1993–18	2400	377	0.009	0.0050	–0.515	–0.523	34.9515	34.9565
1993–22	2400	360	0.010	0.0045	–0.514	–0.524	34.9510	34.9555
1993–24	2400	269	0.010	0.0045	–0.514	–0.524	34.9505	34.9550
1995–44	2480	335	0.010	0.0050	–0.514	–0.524	34.9485	34.9535
1995–47	2500	290	0.010	0.0045	–0.514	–0.524	34.9485	34.9530
1995–50	2450	347	0.010	0.0040	–0.514	–0.524	34.9485	34.9525
2001–44	2400	260	0.011	0.0044	–0.512	–0.523	34.9490	34.9534
2001–45	2350	210	0.011	0.0040	–0.513	–0.524	34.9495	34.9535

D_m is the depth of the potential temperature minimum θ_m (where the salinity is S_m), H is the thickness of the transition layer (between the top of the homogeneous bottom layer and D_m), $\Delta\theta$ and ΔS are the changes in potential temperature and salinity across the transition layer. The homogeneous bottom layer has potential temperature θ_h and salinity S_h . Casts in the near-boundary regions (1993–14, 15 and 1995–57) have been excluded.

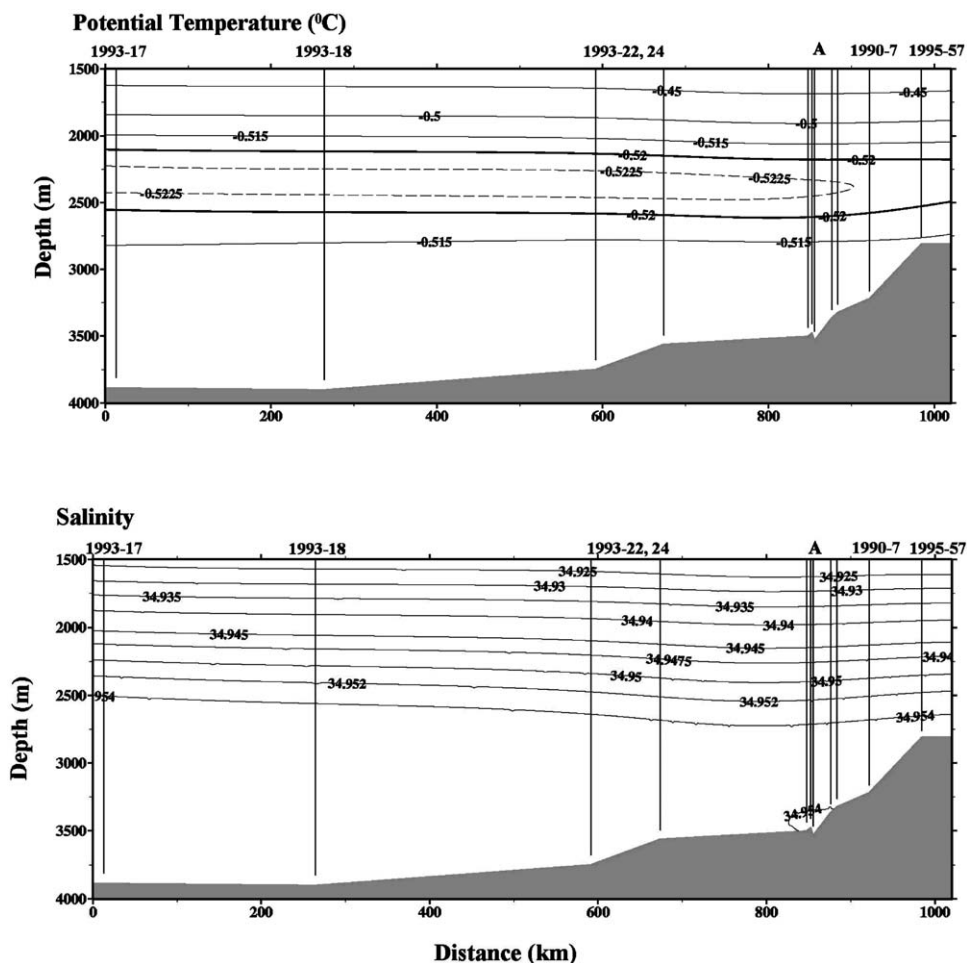


Fig. 3. Vertical sections of potential temperature (top) and salinity (bottom) across the CB along the line shown in Fig. 1.

Profiles of θ and S within the transition layer for every year (between 1990 and 2001) show a striking staircase structure (Figs. 4 and 5) persisting over 11 yr. Each step consists of an *interface* layer within which both θ and S increase with depth, and a *mixed* layer within which both θ and S are uniform. Individual mixed layers appear to be coherent across the CB and over time, however, we do not have sufficient data (nor the resolution or accuracy) to discern lateral or temporal variations of the individual layers. Interface thicknesses are between 2 and 16 m (over which $\delta\theta \approx 0.003^\circ\text{C}$ and $\delta S \approx 0.0007$), while mixed-layer thicknesses are between 10 and 60 m (Table 3). The mixed layers appear as clusters of points in the deep

$\theta - S$ curves in the CB (Fig. 6), rather than as intrusive features. The well-formed staircase is suggestive of double-diffusive processes observed in laboratory experiments of a salinity gradient heated from below (e.g. Turner, 1965).

3. Geothermal heating of the homogeneous bottom layer

The vertical homogeneity of the CB bottom layer, which has a thickness up to 1000 m, suggests that convective mixing is occurring as a consequence of weak geothermal heating. Previously, the geothermally heated bottom layer of the Black

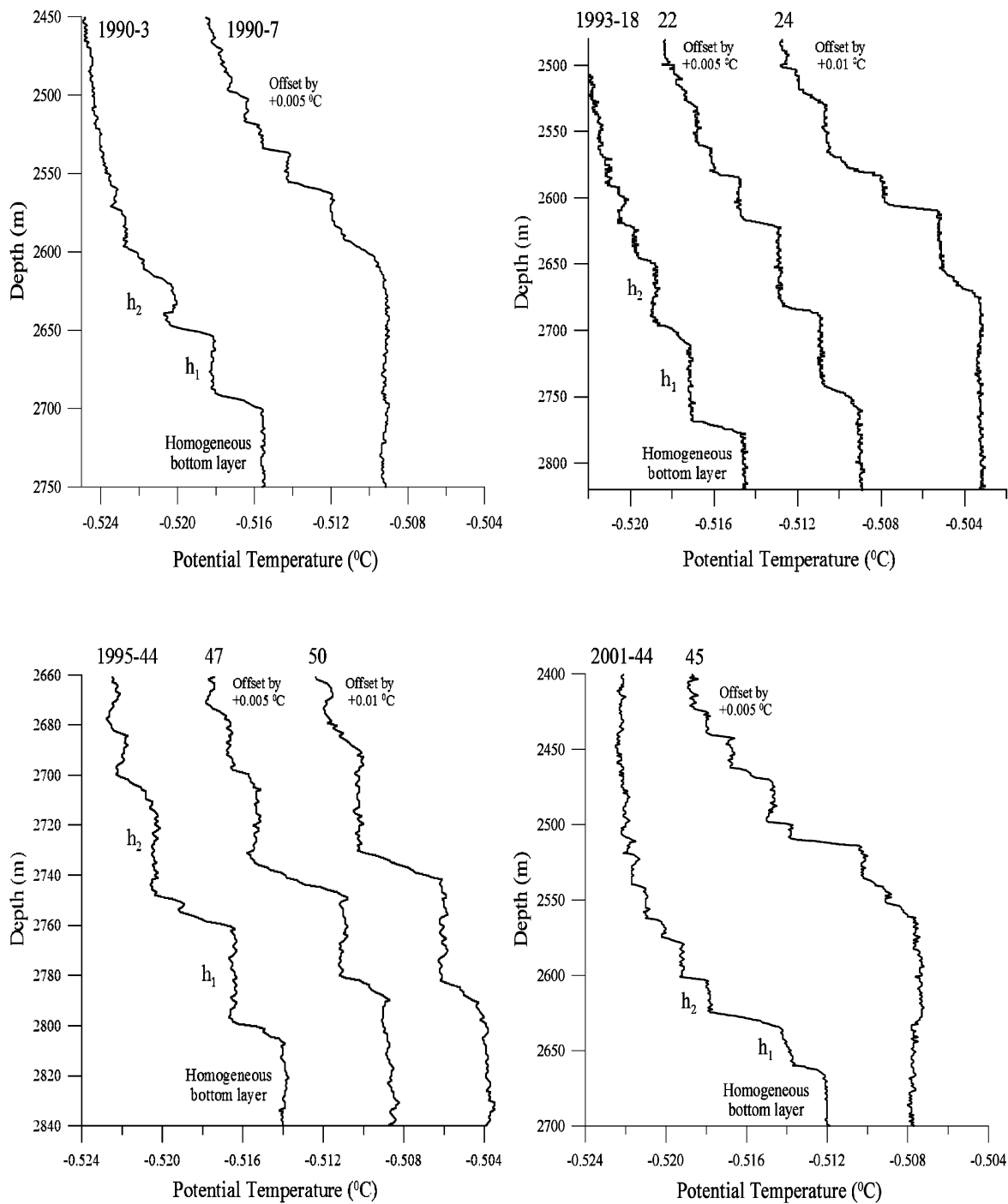


Fig. 4. Profiles of potential temperature in the transition layer in the CB for the casts listed in Table 1 (excluding casts 1993–14, 15 and 1995–57 in the near-boundary region, cast 1993–17, shown in Fig. 5, and cast 1993–9, which had a questionable offset, as shown in Fig. 6).

Sea, with a thickness about 450 m, was recognized as the thickest in the world’s oceans (cf. Kelley et al., 2003).

Langseth et al. (1990) report geothermal heat flux measurements in the CB of 40–60 mW m⁻². These values are based on means of closely

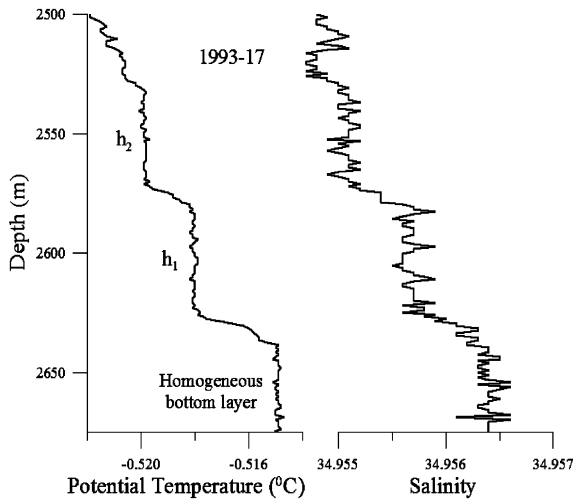


Fig. 5. One example profile of both potential temperature and salinity in the transition layer in the central CB.

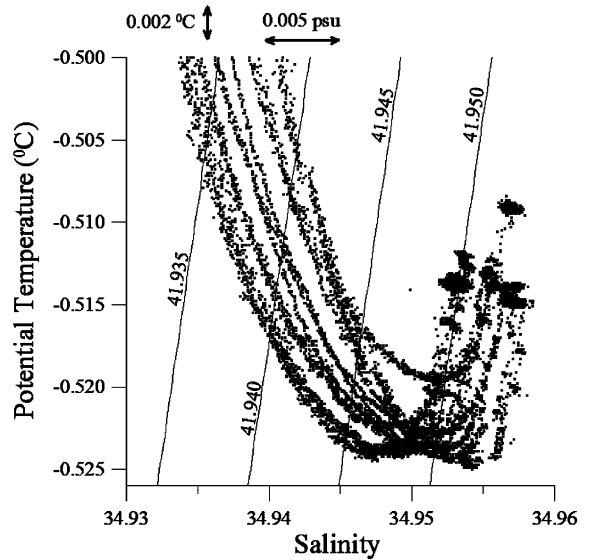


Fig. 6. Potential temperature versus salinity in the deep CB for the casts listed in Table 1 (excluding casts 1993–14, 15 and 1995–57 in the near-boundary region). Isolines of potential density referenced to a pressure of 3000 dbar are also shown. An offset cast (1993–9) is seen by the cluster of points indicating an anomalously warm bottom layer that is associated also with a warmer minimum potential temperature; this is likely due to a calibration error. The bars at the top of the plot indicate the accuracy limitations of the instruments.

Table 3
Characteristics of the staircase

Cast	$\delta h_1, h_1$ (m)	$\delta h_2, h_2$ (m)	$\delta h_3, h_3$ (m)	$\delta \theta_1$ (°C)	$\delta \theta_2$ (°C)	$\delta \theta_3$ (°C)	\bar{R}_ρ	$R_{\rho 1}$	$R_{\rho 2}$	$R_{\rho 3}$
1990–3	10, 38	8, 25		0.003	0.002		1.39	1.06	1.90	
1990–7	13, 28	7, 20	3, 15	0.003	0.002	0.002	1.40	1.06	1.58	1.58
1993–9	14, 30	12, 30		0.003	0.003		1.54	1.81	1.27	
1993–17	10, 45	10, 40		0.003	0.002		1.39	1.27	1.58	
1993–18	10, 60	14, 45	6, 22	0.003	0.002	0.001	2.30	1.52	1.90	5.07
1993–22	12, 55	6, 60	7, 30	0.002	0.002	0.002	1.64	1.27	1.90	1.58
1993–24	16, 45	4, 25	14, 35	0.002	0.003	0.003	1.44	1.27	1.77	1.27
1995–44	8, 40	12, 35		0.003	0.004		1.39	1.52	1.27	
1995–47	10, 35	16, 30		0.002	0.005		1.56	1.90	1.41	
1995–50	12, 45	12, 40		0.002	0.005		1.46	1.58	1.41	
2001–44	7, 25	11, 21	3, 22	0.002	0.004	0.002	1.50	1.58	1.27	1.90
2001–45	10, 15	4, 10	2, 30	0.003	0.004	0.001	1.81	1.58	1.58	3.17

δh_1 is the thickness of the interface between the bottom layer and the first (deepest) mixed layer (of thickness h_1), δh_2 and δh_3 are the interface thicknesses between the first mixed layer and the second (of thickness h_2) and the second mixed layer and the third (of thickness h_3), respectively (similarly for the potential temperature $\delta \theta_n$ and salinity δS_n changes and the density ratio values $R_{\rho n}$). \bar{R}_ρ is calculated using the mean potential temperature and salinity gradients from the top of the homogeneous bottom layer to the top of the shallowest mixed layer in the staircase.

spaced groups of published seafloor heat flow measurements (50 in total) in the Northwest, Central and Southern CB. Furthermore, Langseth et al. (1990) show that the measured geothermal heat flux agrees well with the predicted heat flux for a cooling lithosphere.

If the geothermal heat remains in the bottom layer, this should be observed by an increase in either thickness or temperature of this layer. If all of the geothermal heat ($F_H \approx 50 \text{ mW m}^{-2}$) remains in the bottom layer, the potential temperature θ_h of this layer, of thickness $H \approx 1000 \text{ m}$ (the volume-weighted mean thickness: see, for example, Aagaard et al., 1985), evolves according to $d\theta_h/dt = F_H/(\rho c_p H)$, where $\rho = 1040 \text{ kg m}^{-3}$ is the density and $c_p = 3900 \text{ J kg}^{-1} \text{ }^\circ\text{C}$ is the specific heat of the water. This gives a potential temperature increase of about $0.0004^\circ\text{C yr}^{-1}$, or about 0.004°C between 1990 and 2001. A best fit from all CTD casts over 11 yr indicates a potential temperature increase in the layer of $0.0001 \pm 0.0001^\circ\text{C yr}^{-1}$, implying that no more than about 8 mW m^{-2} remains in this layer. The minimum potential temperature θ_m increases by $0.00002 \pm 0.0001^\circ\text{C yr}^{-1}$. Note that $\theta_h - \theta_m = 0.01 \pm 0.001^\circ\text{C}$ so that it is likely that both θ_m and θ_h remain the same and differences of up to 0.005°C (Fig. 6) in their values from year to year are related to instrument accuracy.

A net increase in heat content of the bottom layer could also be observed as an increase in the thickness of this layer. If 50 mW m^{-2} of geothermal heat remained in the bottom layer (of constant potential temperature), by conservation of heat and given the mean potential temperature gradient in the transition layer $\partial\theta/\partial z \approx 3 \times 10^{-5} \text{ }^\circ\text{C m}^{-1}$, we would observe a 100 m increase in thickness in 1 yr. CTD profiles at station A (1990–3, 1993–9, 1995–44, 47 and 50) can be investigated separately to avoid differences associated with geographic location in the basin. We find that the thickness of the homogeneous layer there decreases by $19 \pm 4 \text{ m yr}^{-1}$ and the depth of θ_m increases by $8 \pm 4 \text{ m yr}^{-1}$. However, a best fit from all CTD casts over 11 yr shows that the bottom layer increases in thickness by $6 \pm 7 \text{ m yr}^{-1}$ and the depth of the minimum potential temperature θ_m decreases by $1 \pm 5 \text{ m yr}^{-1}$. It is thus likely that the thickness of the transition layer does not mono-

tonically increase (or decrease) in time as a result of a net heat flux into the layer. A conservative estimate for the maximum thickness increase that may go undetected would be $\Delta H \approx 20 \text{ m yr}^{-1}$, requiring a heat flux of $F_H \approx 2 \text{ mW m}^{-2}$.

Hence, we can conclude that no more than about 1/5 of the total geothermal heat remains in the bottom layer, as seen by an increase in temperature or thickness of this layer and that there must be some vertical heat flux through the transition layer.

4. Double diffusion

We first hypothesize that the staircase structure of the deep CB (with mixed layers separated by interfaces) is a double-diffusive phenomenon reflecting a destabilizing geothermal heat flux acting against a stable salinity gradient over the long residence time of these waters. In this section, we estimate vertical double-diffusive heat and salt fluxes through the transition layer and compare the heat fluxes to the geothermal heat flux measurements.

The stability of double-diffusive interfaces can be defined in terms of the density ratio $R_\rho = (\beta \delta S)/(\alpha \delta \theta)$, where $\alpha = -\rho^{-1} \partial\rho/\partial T$, $\beta = \rho^{-1} \partial\rho/\partial S$ (density ρ) and $\partial\theta$ and ∂S are the potential temperature and salinity differences across the interfaces (Turner, 1973). R_ρ values for each interface (subscript 1 refers to the deepest interface, 2 to the second deepest and so on) in the CB staircase are $R_{\rho 1} = 1.5 \pm 0.3$, $R_{\rho 2} = 1.6 \pm 0.3$ and $R_{\rho 3} = 2.4 \pm 1.5$, where we have used $\alpha(\theta, p) = 1.2 \times 10^{-4} \text{ }^\circ\text{C}^{-1}$ and $\beta(S, p) = 7.6 \times 10^{-4}$ at $\theta = -0.5^\circ\text{C}$, $S = 34.9$, and pressure $p = 3000 \text{ dbar}$. $\bar{R}_\rho = 1.6 \pm 0.3$ is the mean density ratio over the transition layer. These density ratios are average values over all years and for all casts. There are no discernable trends over time nor in any particular direction.

Laboratory experiments performed by Turner (1965) (and analysed by Huppert, 1971) show that the ratio of fluxes $\gamma = (\beta q_S)/(\alpha q_T)$, where q_S and q_T are the fluxes of salt and temperature, has $\gamma \approx 0.15$ for $2 \leq R_\rho \leq 8$ and $\gamma \rightarrow 1$ as $R_\rho \rightarrow 1$, though the exact form of this transition is not known.

Linden (1974) assumes that the fluxes of heat and salt through the interface when $R_\rho \rightarrow 1$ consist of two additive contributions: a diffusive flux and an entrainment flux resulting from the mechanical mixing through the interface by the interaction of convective motions in the mixed layers. His assumption requires that as $R_\rho \rightarrow 1$ the interfaces no longer have a laminar core. The effects of turbulent entrainment may be significant in the CB where $R_\rho \lesssim 2$.

4.1. Heat fluxes

Many laboratory experiments combined with theoretical analyses and best fits to oceanic situations have addressed the issue of heat fluxes across double-diffusive interfaces. The various formulations produce similar results. Based on comparisons given in the comprehensive review by Kelley et al. (2003), we use the formulation of Kelley (1990) to estimate double-diffusive fluxes through the CB transition layer. The double-diffusive heat flux (in mW m^{-2}) is given by Kelley (1990) as

$$F_H = 0.0032e^{(4.8/R_\rho^{0.72})} \rho c_p \left(\frac{\alpha g \kappa}{Pr} \right)^{1/3} (\delta\theta)^{4/3}, \quad (1)$$

where $Pr = \nu/\kappa$ is the Prandtl number, $\nu = 1.89 \times 10^{-6} \text{ m}^2 \text{ s}^{-1}$ is the kinematic viscosity, $\kappa = 1.28 \times 10^{-7} \text{ m}^2 \text{ s}^{-1}$ is the thermal diffusivity, and $g = 9.81 \text{ m s}^{-2}$. This yields average double-diffusive heat fluxes across the interface between the bottom layer and the first (deepest) mixed layer $F_{H1} = 50 \pm 38 \text{ mW m}^{-2}$, the first mixed layer and the second $F_{H2} = 42 \pm 35 \text{ mW m}^{-2}$, and the second mixed layer and the third $F_{H3} = 22 \pm 20 \text{ mW m}^{-2}$.

The average double-diffusive heat flux, $F_H = 38 \pm 14 \text{ mW m}^{-2}$, is in agreement with geothermal heat flux estimates. This supports the argument that vertical transport across the top of the homogeneous bottom layer is controlled by double diffusion driven by geothermal heat flow. Thus far, we conclude that the step-like structure, values of the stability ratio and double-diffusive heat fluxes in the transition layer in the CB are consistent with double diffusion.

4.2. Salt fluxes

The salt flux q_S through the transition layer can be calculated using the relationship for the ratio of fluxes $\gamma = (\beta q_S)/(\alpha q_T)$. Hence, for $R_\rho > 2$ ($\gamma \approx 0.15$), $q_S \approx 3 \times 10^{-10} \text{ m s}^{-1}$, and for $R_\rho \rightarrow 1$ ($\gamma \rightarrow 1$), $q_S \approx 2 \times 10^{-9} \text{ m s}^{-1}$ (we have taken $F_H = \rho c_p q_T \approx 50 \text{ mW m}^{-2}$). By conservation of salt in the bottom homogeneous layer, $dS_h/dt = -q_S/H$ where $H \approx 1000 \text{ m}$. Hence, the double-diffusive salt flux should result in a decrease of the lower layer salinity of between $1 \times 10^{-5} \text{ yr}^{-1}$ ($\gamma = 0.15$) and $6 \times 10^{-5} \text{ yr}^{-1}$ ($\gamma = 1$), or between about 0.0001 and 0.001 over 11 yr. Best fits of CTD data show that both the salinity of the bottom layer and the salinity at the depth of θ_m decrease by $0.0004 \pm 0.0007 \text{ yr}^{-1}$ or about 0.004 ± 0.007 over 11 yr. Hence, salt flux calculations are not ruled out by the data, although they are not confirmed. Eleven year changes are the same order of magnitude as accuracy limitations (0.002–0.005) of the instrument. The implications of the predicted salt fluxes will be discussed in Section 7.

4.3. Mixed-layer thicknesses

We have hypothesized that the observed staircase structure arises from double-diffusive convection and obeys laboratory flux laws. We may check this hypothesis by comparing the observed and expected thicknesses of the layers and interfaces using relationships found in previous studies of diffusive systems.

The first mixed layer above the homogeneous bottom layer in the CB has thickness $h_1 = 40 \pm 10 \text{ m}$, the second mixed layer has $h_2 = 33 \pm 11 \text{ m}$ and the third mixed layer has $h_3 = 25 \pm 7 \text{ m}$.

Kelley (1984) was the first to propose a parameterization for the characteristic mixed-layer thickness h in a double-diffusive staircase. He uses dimensional analysis to derive an expression for layer thickness and he suggests that this scaling holds because h is controlled by a balance between mixed-layer merging and interface splitting, whereby new layers are formed from existing interfaces. Observations in various ocean and lake regions are in reasonable agreement (Kelley et al., 2003).

We calculate a representative mixed-layer thickness h for the deep CB using the parameterization of Kelley (1984) given by

$$h \approx (\kappa/\bar{N})^{1/2} [0.25 \times 10^9 \bar{R}_\rho^{1.1} Pr(\bar{R}_\rho - 1)]^{1/4} \approx 6 \pm 1 \text{ m}, \quad (2)$$

where $\bar{N} = [g(\alpha \overline{\partial\theta/\partial z} - \beta \overline{\partial S/\partial z})]^{1/2} \approx 2 \times 10^{-4} \text{ s}^{-1}$ is the buoyancy frequency and $\bar{N}_s = (g\beta \overline{\partial S/\partial z}) \approx 3 \times 10^{-4} \text{ s}^{-1}$. Hence, mixed-layer thicknesses in the CB are about five times thicker than the characteristic thickness resulting from the quasi-empirical relationship proposed by Kelley (1984). Discrepancies between theory and observation also arise with respect to interface thicknesses.

4.4. Interface thicknesses

The interfaces between convective layers in the CB are between 2 and 16 m thick. Double-diffusive heat fluxes can be compared with the molecular transport through these high-gradient interfaces. If the core regions of the interfaces are always laminar (i.e. in the absence of turbulent mixing), then the conductive heat flux can be estimated by $F_M = \rho c_p \kappa \partial T/\partial z$ across interfaces. Here $\partial T/\partial z \approx 3 \times 10^{-4} \text{ }^\circ\text{C m}^{-1}$ is the in situ temperature gradient between the homogeneous bottom layer and the overlying mixed layer. This yields $F_M \approx 0.2 \text{ mW m}^{-2}$, or about 250 times less than both the double-diffusive and geothermal heat flux estimates. Similarly, the conductive heat flux across the interface between the first and the second mixed layers is $F_M \approx 0.1 \text{ mW m}^{-2}$.

The interfaces in the CB are thus too thick to support the required heat flux by molecular conduction. For the observed potential temperature step $\delta\theta \approx 0.003^\circ\text{C}$, and a geothermal heat flux $F_H = 40\text{--}60 \text{ mW m}^{-2}$, the required thickness of the interfaces is about 2–4 cm. There remains the possibility that there are unresolved mixed layers within the observed interfaces (the sandwich layers described by Kelley, 1988). We use the resolution limits of the instruments to estimate the possible thickness of such layers should they exist. The hydrographic data were collected at CTD descent rates between 0.5 and 1.5 m s^{-1} at sampling rates between 2 and 24 Hz, which would permit the

resolution of interfaces between 2.5 and 75 cm thick. This is not limited by temperature probe response times, which were between 0.07 and 0.4 s, yielding response lengths of 4–40 cm. (It is important to note that turbulence around the profiling instrument does not play a significant role; for example, there are no observed differences in interface structure between up and down casts.) Hence, a conservative estimate for the thickness of unresolved layers would be $\lesssim 2$ m. The existence of such structure would lead to very different heat fluxes. The average interface thickness in the CB staircase is $\delta h \approx 10$ m. Hence, if there were unresolved mixed layers (approximately 2 m thick) within the interfaces, then by the 4/3 flux laws, the heat flux would be reduced by $(1/5)^{4/3} \approx 0.1$. This would give a heat flux through the transition layer of about 5 mW m^{-2} , much less than the geothermal heat flux.

It is possible that the interface cores are non-laminar because of increased interfacial entrainment when $R_\rho \rightarrow 1$, or as a result of externally driven turbulence, or both. In any case, a larger diffusivity (a turbulent diffusivity κ_z) is required in the interfaces in order to support the predicted heat flux through them.

5. Is there turbulent mixing in the staircase interfaces?

We can estimate a turbulent vertical diffusivity κ_z in the interfaces by dividing geothermal temperature fluxes by the potential temperature gradients $\partial\theta/\partial z$ in the interfaces. That is, $\kappa_z = F_H(\rho c_p \partial\theta/\partial z)^{-1} \approx 4 \times 10^{-5} \text{ m}^2 \text{ s}^{-1}$, for $\partial\theta/\partial z \approx 3 \times 10^{-4} \text{ }^\circ\text{C m}^{-1}$ and $F_H \approx 50 \text{ mW m}^{-2}$.

5.1. Thorpe scale

We could verify the estimated value of κ_z by observing mixing indicated by unstable regions in density profiles in the interfaces (Thorpe, 1977). The Thorpe scale L_T is defined as the root mean square of the vertical displacements (Thorpe displacements) required to reorder the profile of potential density so that it is gravitationally stable. It is thought to be related to the Ozmidov scale,

$L_O = (\varepsilon/N^3)^{1/2}$, where ε is the dissipation rate of kinetic energy. Dillon (1982) finds $L_O \approx 0.8L_T$, so that, with $\kappa_z \approx 0.2\varepsilon/N^2 = 0.2L_O^2N$ (Oakey, 1982), the vertical diffusivity is given in terms of the Thorpe scale by $\kappa_z \approx 0.1NL_T^2$. Here $N \approx 3.5 \times 10^{-4} \text{ s}^{-1}$ in the interfaces, so that, for $\kappa_z \approx 4 \times 10^{-5} \text{ m}^2 \text{ s}^{-1}$, $L_T \approx 1 \text{ m}$.

The salinity data are not sufficiently resolved for us to use the density profiles, but we look for Thorpe displacements in the potential temperature profiles. These displacements are an indication of mixing if they are not due to intrusions or noise. Thorpe displacements have values that range from zero to many times L_T (Galbraith and Kelley, 1996; Stansfield et al., 2001).

A typical potential temperature profile (1993–17, Fig. 7) illustrates fluctuations from a stable profile in an interface separating a cool mixed layer from a warmer mixed layer below. We rule out the possibility of unstable potential temperatures caused by salinity-compensated intrusions; such intrusions would easily be eradicated by diffusion over the horizontal distance that they would have to be coherent (about 100 km). However, the displacements may be an indication

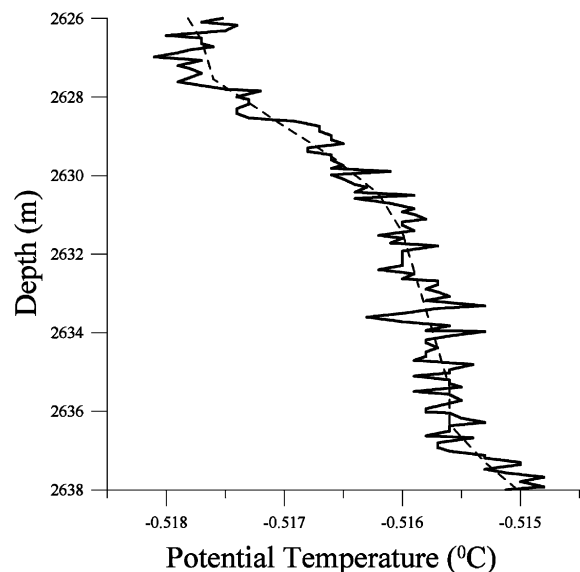


Fig. 7. Typical profile of potential temperature in an interface separating two mixed layers (cast 1993–17). The meter-averaged profile (dotted line) is also shown.

of instrument noise. For example, visual inspection of the interface profile suggests that reordering regions might result from random potential temperature perturbations with short runs of alternating positive and negative displacements. This is in contrast to real Thorpe displacements, which have long runs (run lengths).

Following Galbraith and Kelley (1996), we have computed Thorpe scales in two typical profiles of potential temperature in interfaces. To investigate the effects of instrument noise on Thorpe displacements, we modified the re-sorted profiles by adding random noise from a normal distribution having an rms value approximately equal to the instrument resolution, 0.0004°C , and computed Thorpe scales L_{TN} . The Thorpe scales L_T are approximately equal to L_{TN} (Table 4), suggesting that the displacements in the interface profiles are indeed a result of noise. We computed the rms run length for each potential temperature profile as well as for the re-sorted profiles with added noise. As explained by Galbraith and Kelley (1996), for random noise the probability of a run of length n is 2^{-n} . Hence, the rms run length is $(\sum_1^\infty 2^{-n}n^2)^{1/2} = \sqrt{6} \approx 2.45$. The rms run lengths of the profiles are not significantly higher than rms run lengths from noise, which are close to the theoretical limit. We conclude that the observed displacements are not statistically significant and cannot reasonably be attributed to mixing.

Bounds on measurable signals prevent us from completely ruling out the possibility that the required Thorpe scales exist. However, it does seem that we would need to see more larger

Table 4

Thorpe scales L_T computed over two typical profiles of potential temperature in an interface. Interface 1 is shown in Fig. 7

Interface	L_T (m)	L_{TN} (m)	rms run length	rms run length N
1	1.4	1.8	3.1	2.5
2	0.7	0.8	3.2	2.4

L_{TN} is the Thorpe scale of the re-sorted interface profile with added random noise having an rms value of 0.0004°C (L_{TN} is computed over 1000 realizations). The run lengths in the fourth and fifth columns are for the profile and the re-sorted profile with added noise respectively.

displacements and longer runs in typical profiles of potential temperature in the interfaces if the diffusivity was sufficient to support the geothermal heat flux through them. Hence, we can likely discount the possibility of a heat flux comparable with the geothermal flux.

5.2. Interface maintenance

While it is clear that the vertical heat flux through the interfaces is not as large as the measured geothermal heat flux, the vertical fluxes must still be sufficient to maintain the mixed-layers and interfaces. The latter would otherwise be thickened by conduction with sharp interfaces becoming approximately $2\sqrt{\kappa t}$ thick in time t . Hence, in 10 yr, an interface between convective layers becomes about 13 m thick by molecular diffusion alone. However, we observe that mean interface thicknesses were 8 ± 3 m in 1990, 10 ± 3 m in 1993, 11 ± 2 m in 1995 and 6 ± 3 m in 2001, suggesting that the effects of molecular conduction are offset by maintenance of the structure by double diffusion, although with a smaller heat flux than the measured geothermal heat flux. The structure can be maintained at smaller heat fluxes because thicker interfaces grow more slowly by conduction, so that even weaker convective entrainment velocities (possibly proportional to the vertical buoyancy flux to the 1/3 power (Turner, 1973), will preserve the interfaces.

6. How is the geothermal heat escaping?

There is no evidence of bottom-layer warming or thickening. Moreover, it seems that the total geothermal heat cannot be transported through the staircase interfaces. However, we observe that well-mixed layers are absent near the edge of the CB (Fig. 8) near the 3000 m isobath, suggesting increased mixing there. In this section, we investigate whether there is a higher vertical heat flux at the basin boundaries, assuming that there is some lateral circulation in the well-mixed bottom layer in order to supply this vertical heat flux near the boundaries.

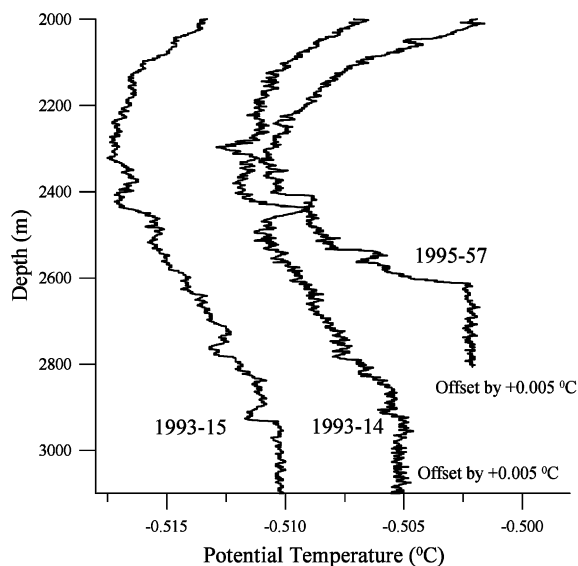


Fig. 8. Profiles of potential temperature at the boundaries of the CB.

An effective diffusivity K_z (for use in models that do not resolve the mixed layers, for example) can be computed by dividing temperature fluxes by temperature gradients smoothed over the transition layer. That is, $K_z = F_H / (\rho c_p \overline{\partial\theta/\partial z})$, where $\overline{\partial\theta/\partial z} \approx 3 \times 10^{-5} \text{ } ^\circ\text{C m}^{-1}$ (a mean over the transition layer) in the CB. The predicted vertical heat flux of about 50 mW m^{-2} out of the bottom layer (through the transition layer) yields $K_z \approx 4 \times 10^{-4} \text{ m}^2 \text{ s}^{-1}$.

To assess the fraction of the basin over which near-boundary mixing might occur, we examine the distance from lateral boundaries at which staircases are absent below the depth of the potential temperature minimum. We do not observe the staircase structure where the bottom depth is less than about 500 m below the depth of θ_m . Hence, we estimate the area of a horizontal slice through the transition layer in regions where it is less than 500 m to the bottom. This total area will vary depending upon the bottom slope, but a rough estimate yields approximately 35% of the total area of the CB. Therefore, the appropriate vertical diffusivity required near the boundaries is $\kappa_b \approx K_z / 0.35 \approx 1 \times 10^{-3} \text{ m}^2 \text{ s}^{-1}$. While this estimate of diffusivity κ_b seems high, the dissipation rate of kinetic energy, given by $\varepsilon \approx 5\kappa_b \overline{N^2} \approx 2 \times$

$10^{-10} \text{ W kg}^{-1}$, where $\overline{N^2} = 4 \times 10^{-8} \text{ s}^{-2}$ in the transition layer, is small in this region of very weak stratification.

This estimated dissipation rate is small compared with that observed in other abyssal regions. In the deep Brazil Basin, for example, values of several times $10^{-9} \text{ W kg}^{-1}$ were found within a few hundred meters of the bottom (at about 4000 m) over rough topography, though the dissipation levels higher up in the water column and over smooth topography were only a few times $10^{-10} \text{ W kg}^{-1}$ (Polzin et al., 1997). We may pursue the energy requirements further by noting that the basin average requirement, as opposed to that in the limited boundary regions, is about $7 \times 10^{-11} \text{ W kg}^{-1}$. Multiplying by the 300 m thickness of the transition layer, and the density of water, this would require a surface energy input of about 0.02 mW m^{-2} . To be precise, one should add about 20% to allow for the buoyancy flux, thus obtaining closer to 0.03 mW m^{-2} . This is much less than the 1 mW m^{-2} global average input to wind-driven inertial waves (Alford, 2001), though, in the Arctic, ice cover may inhibit the generation of such motions. Halle and Pinkel (2003) have found a downward energy flux of no more than 0.1 mW m^{-2} beneath ice cover at the western side of the CB. More energy may come in from seasonal open water areas, and some mixing may be caused by tidal motions. Part of the CB is located above the critical latitude (74.5°) for the M_2 tide wave, while the S_2 tide propagates freely; maximum tidal currents in the CB are between about 5 and 10 cm s^{-1} and there is also evidence for topographically amplified diurnal tidal currents (see for example, Kowalik et al., 2002). We

conclude that the large mixing rate required may be energetically possible.

In this scenario, it must be assumed that some lateral flux takes place in the bottom layer to sustain the enhanced flux at the boundaries. Furthermore, above the depth of θ_m , the water is no longer confined to the basin; we assume that lateral processes here can transport the flux from the boundary regions.

6.1. Thorpe scale

The Thorpe scale corresponding to the required vertical diffusivity near the boundaries is $L_T \approx \sqrt{\kappa_b} (0.1 \sqrt{N^2})^{-1/2} \approx 7 \text{ m}$. The signals are large so we have chosen to work with 1 m-averaged data. In this case the noise is reduced from about 0.0004°C to $0.0004/\sqrt{24}^\circ\text{C}$ for 24 Hz data and a CTD descent rate of 1 m s^{-1} . We have computed Thorpe scales on potential temperature profiles in the transition layer for each of the three boundary casts (Table 5). In addition, we calculated L_{TN} for the re-sorted profiles with added random noise having an rms value of $0.0004/\sqrt{24}^\circ\text{C}$. In these boundary profiles, unlike for the interface profiles, we find that the addition of noise to the re-sorted profiles yields Thorpe scales that are smaller than the Thorpe scales of the original profiles.

Again, we have computed rms run lengths on re-sorted profiles. The rms run length of each profile is about twice the rms run length of each re-sorted, noise-added profile, which again, is close to the theoretical limit of about 2.4. This leads us to believe that the observed displacements in the

Table 5
Thorpe scales L_T computed over the given depth ranges

Cast	Depth range (m)	L_T (m)	L_{TN} (m)	rms run length	rms run length N
1993–14	2450–2750	16	7	4.3	2.2
1993–15	2400–2700	18	9	4.4	2.3
1995–57	2400–2550	12	6	4.5	2.2

L_{TN} is the Thorpe scale of the re-sorted profile with added random noise having an rms value of $0.0004/\sqrt{24}^\circ\text{C}$ (L_{TN} is computed over 1000 realizations). The run lengths are for the profile and the re-sorted profile with added noise. The run lengths in the fifth and sixth columns are for the profile and the re-sorted profile with added noise respectively.

boundary profiles can reasonably be attributed to mixing though it is difficult to be precise about the value of κ_b .

There remains the possibility that intrusions influence the calculations. For example, the potential temperature fluctuations associated with Thorpe displacements, typically $\lesssim 0.0005^\circ\text{C}$, would be compensated by a change in salinity of 8×10^{-5} , which we cannot measure because of inadequate salinity resolution. Such intrusions would have to be coherent over a horizontal distance of between 10 and 20 km, which is not impossible for features that would have thicknesses around 10 m.

7. Deep-water renewal scenarios

We have so far assumed that the CB deep water was formed around 500 years ago (based on the ^{14}C isolation age estimates) and that there is presently a balance between geothermal heat flux and diffusive heat loss. In this scenario the salt content of the bottom homogeneous layer, of average thickness $H \approx 1000$ m, evolves according to $dS_h/dt = -(K_z/H)\partial S/\partial z$, where $\partial S/\partial z \approx 1 \times 10^{-5} \text{ m}^{-1}$ is the mean salinity gradient over the transition layer. Hence, the salt content of the bottom layer decreases by about $1 \times 10^{-4} \text{ yr}^{-1}$ and the salinity of the bottom water would have been about 35 after the basin was last ventilated. Furthermore, if the vertical transport of salt were to continue through the top of the transition layer, at about 2400 m, the salt would become uniform from this depth to the bottom about 40 yr from now and there would be no staircase structure in the transition layer.

A different scenario involves the renewal of some fraction ϕ of salt (of salinity ΔS (positive) more than the bottom-layer salinity) per year. Conservation of salt in this scenario can be expressed as $\phi H \Delta S = K_z \partial S/\partial z$. Based on ^{14}C isolation ages of the bottom homogeneous layer, we take the average age of the CB deep water to be 500 years (Schlosser et al., 1997; Macdonald et al., 1993). Hence, assuming the incoming water mixes with its surroundings, $\phi = 1/500 \text{ yr}^{-1}$. This requires $\Delta S \approx 0.066$. On the other hand, the deriva-

tion of K_z effectively assumes that there is no potential temperature difference $\Delta\theta$ between the incoming and bottom water. For the more realistic situation in which both ΔS and $\Delta\theta$ are non-zero, the vertical diffusivity K_z must vary. We must therefore consider a more general model.

The conservation equations for salt and potential temperature in the bottom layer are given by

$$H\partial\theta/\partial t - H\phi\Delta\theta - F_H/(\rho c_p) = -K_z\partial\theta/\partial z \quad (3)$$

$$H\partial S/\partial t - H\phi\Delta S = -K_z\partial S/\partial z \quad (4)$$

① ② ③ ④

where $\Delta\theta$ is the potential temperature of the incoming water minus the potential temperature of the homogeneous bottom layer.

In Sections 1–6 we have considered the case where there a balance between terms ③ and ④ in Eq. (3) and a balance between terms ① and ④ in Eq. (4). We now consider a general steady-state scenario and we neglect term ① in both equations and introduce term ②. If the geothermal heat flow into the bottom layer is used entirely to heat this layer (i.e. no heat flux through the transition layer, $K_z = 0$) then the incoming water is colder than this layer by an amount $\Delta\theta \approx -0.2^\circ\text{C}$ (where we have taken the geothermal heat flux to be 50 mW m^{-2}

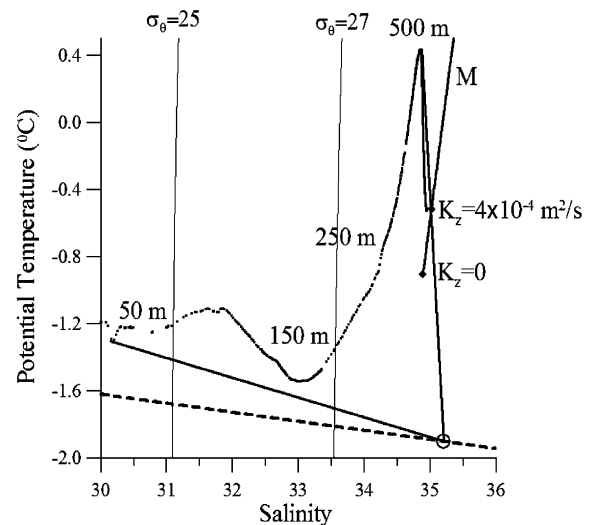


Fig. 9. Potential temperature vs. salinity in the deep CB. Cold saline shelf water is shown by the open circle on the dashed freezing line. Line M is drawn from Eq. (5).

and again, $\phi = 1/500 \text{ yr}^{-1}$). This is a limiting case. Alternatively, the turbulent heat flux through the transition layer is less than the geothermal heat flux into the bottom layer (i.e. only some geothermal heat is used in heating incoming cold water and $K_z < 4 \times 10^{-4} \text{ m}^2 \text{ s}^{-1}$). We combine Eqs. (3) and (4) to yield

$$(0.2 + \Delta\theta)/(\overline{\partial\theta/\partial z}) = \Delta S/(\overline{\partial\theta/\partial z}), \quad (5)$$

shown by line M in Fig. 9. This raises the question as to what point on line M is likely to describe renewing water.

We hypothesize that shelf water at the freezing point constitutes the major salt source for the deep water and we test this hypothesis in the context of our renewal scenario. This is the simplest case, and does not consider deep-water renewal by flows over the deep ridges (or through gaps in the ridges) from adjacent basins, as discussed at the end of this section.

Weingartner et al. (1998) observe water having a maximum salinity of 35.2 in the Chukchi Sea; they suggest that these dense shelf waters could penetrate deeper than the halocline. Water overlying the southeastern shelf of the CB can have salinities between 33 and 35 during some winters (Melling, 1993). As an example, we take cold shelf water at the freezing point having a salinity of 35.2 that mixes successively with waters at intermediate depths in the CB, so that the CB deep water is a linear mixture of source and intermediate water.

Dense water that reaches the deep basin must lie somewhere in the sector defined by the source water and lines to the $\theta - S$ curve for the whole water column. The product must, of course, also be at least as dense as the present bottom water. In practice, given the small influence on density of the temperature, we effectively require the renewing water to be at least as salty as the present bottom water.

Our model also requires that the renewing water be on line M. Inspection of Fig. 9 shows that, to satisfy these requirements, the renewing water is likely to be at the lower end of line M, implying vertical diffusivities considerably less than $4 \times 10^{-4} \text{ m}^2 \text{ s}^{-1}$.

In summary, if shelf water does reach the deep, having mixed with the intermediate waters, the

more likely steady-state scenario tends towards cold water ($\Delta\theta \gtrsim -0.2^\circ\text{C}$) renewing the bottom layer, which is then slowly geothermally heated, while the vertical heat and salt fluxes through the top of the transition layer are small (i.e. only the small fluxes required to maintain the staircase structure).

The possibility that the deep waters of the CB are renewed by an influx of water from the Makarov Basin over the Alpha-Mendeleev Ridge remains open to discussion and requires an analysis of the hydrographic data in the Makarov Basin. Given that there are no other outlets for the CB deep water, it is important that any water that is postulated as a candidate for renewal must be at least as dense as the water that it is displacing. While our model does not specify the relative importance of the various sources for the deep water, as investigated for example by Rudels (1986), Rudels et al. (1994) and Jones et al. (1995), Eqs. (3) and (4) can be used to test the likelihood of alternative renewal scenarios.

8. Discussion

Our present preferred interpretation of the thermohaline structure and evolution of the CB deep water may be summarized as follows:

- (1) The present deep water was created approximately 500 years ago and there is no ongoing renewal.
- (2) The geothermal heat flux has warmed this water and played a role in establishing the staircase structure observed above the thick bottom layer.
- (3) The vertical heat flux through the staircase is small, with most of the geothermal heat escaping in regions near the boundaries where the staircase is not observed and there is some evidence for strong vertical mixing.
- (4) The excess salinity of the deep water is decreasing and will vanish within a few decades. That is, the salinity in the CB will be uniform, having its present value at the depth of the potential temperature minimum, from this depth to the bottom.

We must admit, however, that the evidence for all of these points is incomplete. We have thus briefly explored a class of alternative scenarios involving some ongoing renewal of the bottom water. In such a situation, part of the geothermal heat flux would be needed just to heat the new water, so that there will be less vertical heat flux.

We have not explored the lateral structure of the layers, nor have we explored lateral mixing processes, which likely influence the deep thermohaline structure.

Further observational programs are therefore desirable to look for bottom-water renewal and to use other techniques (for example, microstructure or tracers) to assess mixing rates in the interior and near-boundary regions of the basins. These in turn will help guide theoretical models of the various vertical and lateral processes that maintain the remarkable staircase structure.

Acknowledgements

We acknowledge the technical support teams of Arctic-1990–2001, as well as the officers and crew of the CCGS *Henry Larsen*, the USCG *Polar Star*, the CCGS *Louis S. St-Laurent*, and the CCGS *Sir Wilfred Laurier*. Special thanks to Ron Perkin for his collection of the 1993 data and helpful input. We thank Dan Kelley and other, anonymous, reviewers for comments on a different manuscript on the deep CB, and reviewers of the present paper for their comments. Thanks also to Conor Shaw for performing the Thorpe scale computations. The support of the US Office of Naval Research and the Natural Sciences and Engineering Research Council, Canada, is also gratefully acknowledged.

References

- Aagaard, K., Carmack, E.C., 1994. The Arctic Ocean and climate: a perspective. In: Johannessen, O.M., Muench, R.D., Overland, J.E. (Eds.), *The Polar Oceans and Their Role in Shaping the Global Environment*. Geophysics Monographs 85. American Geophysical Union, Washington, DC, pp. 5–20.
- Aagaard, K., Swift, J.H., Carmack, E.C., 1985. Thermohaline circulation in the arctic Mediterranean seas. *Journal of Geophysical Research* 90, 4833–4846.
- Alford, M.H., 2001. Internal swell generation: the spatial distribution of energy flux from the wind to mixed-layer near-inertial motions. *Journal of Physical Oceanography* 31, 2359–2368.
- Dillon, T.M., 1982. Vertical overturns: a comparison of Thorpe and Ozmidov scales. *Journal of Geophysical Research* 87, 9601–9613.
- Galbraith, P.S., Kelley, D.E., 1996. Identifying overturns in CTD profiles. *Journal of Atmospheric and Oceanic Technology* 13, 688–702.
- Halle, C., Pinkel, R., 2003. Internal wave variability in the Beaufort Sea during the winter of 1993/94. *Journal of Geophysical Research* 108, No. C7, 3210, doi:10.1029/2000JC000703.
- Huppert, H.E., 1971. On the stability of a series of double-diffusive layers. *Deep-Sea Research I* 18, 1005–1021.
- Jones, E.P., Rudels, B., Anderson, L.G., 1995. Deep waters of the Arctic Ocean: origins and circulation. *Deep-Sea Research I* 42, 737–760.
- Kelley, D.E., 1984. Effective diffusivities within oceanic thermohaline staircases. *Journal of Geophysical Research* 89, 10484–10488.
- Kelley, D.E., 1988. Explaining effective diffusivities within diffusive oceanic staircases. In: Nihoul, J.C.J., Jamart, B.M. (Eds.), *Small-Scale Turbulence and Mixing in the Ocean*. Elsevier, Amsterdam, pp. 481–502.
- Kelley, D.E., 1990. Fluxes through diffusive staircases: a new formulation. *Journal of Geophysical Research* 95, 3365–3371.
- Kelley, D.E., Fernando, H.J.S., Gargett, A.E., Tanny, J., Özsoy, E., 2003. The diffusive regime of double-diffusive convection. *Progress in Oceanography* 56, 461–481.
- Kowalik, Z., Proshutinsky, A., Thomas, R.H., 2002. Investigation of the ice-tide interaction in the Arctic Ocean. WWW Page, <http://www.ims.alaska.edu:8000/tide/index.html>
- Langseth, M.G., Lachenbruch, A.H., Marshall, B.V., 1990. Geothermal observations in the Arctic region. In: Grantz, A., Johnson, L., Sweeney, J.F. (Eds.), *The Geology of North America, The Arctic Ocean Region*. Geological Society of America, Boulder, CO, pp. 133–151.
- Linden, P.F., 1974. A note on the transport across a diffusive interface. *Deep-Sea Research I* 21, 283–287.
- Macdonald, R.W., Carmack, E.C., 1991. Age of Canada basin deep waters: a way to estimate primary production for the Arctic Ocean. *Science* 254, 1348–1350.
- Macdonald, R.W., Carmack, E.C., Wallace, D.W.R., 1993. Tritium and radiocarbon dating of Canada basin deep waters. *Science* 259, 103–104.
- Melling, H., 1993. The formation of a haline shelf front in wintertime in an ice-covered Arctic Sea. *Continental Shelf Research* 13, 1123–1147.
- Oakey, N.S., 1982. Determination of the rate of dissipation of turbulent energy from simultaneous temperature and

- velocity shear microstructure measurements. *Journal of Physical Oceanography* 12, 256–271.
- Östlund, H.G., Possnert, G., Swift, J.H., 1987. Ventilation rate of the deep Arctic Ocean from carbon 14 data. *Journal of Geophysical Research* I 93, 3769–3777.
- Perry, R.K., Fleming, H.S., 1986. Bathymetry of the Arctic Ocean. The Geological Society of America, Boulder, CO.
- Polzin, K.L., Toole, J.M., Ledwell, J.R., Schmitt, R.W., 1997. Spatial variability of turbulent mixing in the abyssal ocean. *Science* 276, 93–96.
- Rudels, B., 1986. The theta-S relations in the northern seas: Implications for the deep circulation. *Polar Research* 4, 133–159.
- Rudels, B., Jones, E.P., Anderson, L.G., Kattner, G., 1994. On the intermediate depth waters of the Arctic Ocean. In: Johannessen, O.M., Muench, R.D., Overland, J.E. (Eds.), *The Polar Oceans and Their Role in Shaping the Global Environment: The Nansen Centennial Volume*. Geophysical Monograph 85. American Geophysical Union, Washington, DC, pp. 33–46.
- Rudels, B., Muench, R.D., Gunn, J., Shauer, U., Friedrich, H.J., 2000. Evolution of the Arctic Ocean boundary current north of the Siberian shelves. *Journal of Marine Systems* 25, 77–99.
- Schlosser, P., Kromer, B., Ekwurzel, B., Bönisch, G., McNichol, A., Schneider, R., von Reden, K., Östlund, H.G., Swift, J.H., 1997. The first trans-arctic ¹⁴C section: comparison of the mean ages of the deep waters in the Eurasian and Canadian basins of the Arctic Ocean. *Nuclear Instruments and Methods B* 123 (1–4), 431–437.
- Stansfield, K., Garrett, C., Dewey, R., 2001. The probability distribution of the Thorpe displacement within overturns in Juan de Fuca Strait. *Journal of Physical Oceanography* 31, 3421–3434.
- Swift, J.H., Jones, E.P., Aagaard, K., Carmack, E.C., Hingston, M., Macdonald, R.W., McLaughlin, F.A., Perkin, R.G., 1997. Waters of the Makarov and Canada basins. *Deep-Sea Research I* 44, 1503–1530.
- Thorpe, S.A., 1977. Turbulence and mixing in a Scottish Loch. *Philosophical Transactions of the Royal Society London* 286A, 125–181.
- Turner, S.D., 1965. The behavior of a stable salinity gradient heated from below. *Journal of Fluid Mechanics* 33, 183–200.
- Turner, S.D., 1973. *Buoyancy Effects in Fluids*. Cambridge University Press, Cambridge.
- UNESCO, 1983. Algorithms for computation of fundamental properties of seawater. UNESCO Technical Papers Marine Science, 44.
- Weingartner, T.J., Cavalieri, D.J., Aagaard, K., Sasaki, Y., 1998. Circulation, dense water formation, and out flow on the northeast Chukchi shelf. *Journal of Geophysical Research* 103 (C4), 7647–7661.